

# Constraints on Models for TeV Gamma Rays from Gamma-Ray Bursts

P. Chris Fragile\*

*University of California, Lawrence Livermore National Laboratory, Livermore, CA 94550*

Grant J. Mathews and John Poirier

*University of Notre Dame, Center for Astrophysics,*

*Department of Physics, Notre Dame, IN 46556*

Tomonori Totani

*Theory Division, National Astronomical Observatory, Mitaka, Tokyo, 181-8588, Japan*

arXiv:astro-ph/0206383v3 5 Sep 2003

## Abstract

We explore several models which might be proposed to explain recent possible detections of high-energy (TeV) gamma rays in association with low-energy gamma-ray bursts (GRBs). Likely values (and/or upper limits) for the source energies in low- and high-energy gamma rays and hadrons are deduced for the burst sources associated with possible TeV gamma-ray detections by the Project *GRAND* array. Possible spectra for energetic gammas are deduced for three models: 1) inverse-Compton scattering of ambient photons from relativistic electrons; 2) proton-synchrotron emission; and 3) inelastic scattering of relativistic protons from ambient photons creating high-energy neutral pions, which decay into high-energy photons. These models rely on some basic assumptions about the GRB properties, e.g. that: the low- and high-energy gamma rays are produced at the same location; the time variability of the high-energy component can be estimated from the FWHM of the highest peak in the low-energy gamma ray light curve; and the variability-luminosity relation of Fenimore & Ramirez-Ruiz (2000) gives a reliable estimate of the redshifts of these bursts. We also explore the impact of each of these assumptions upon our models. We conclude that the energetic requirements are difficult to satisfy for any of these models unless, perhaps, either the photon beaming angle is much narrower for the high-energy component than for the low-energy GRB or the bursts occur at very low redshifts ( $\lesssim 0.01$ ). Nevertheless, we find that the energetic requirements are most easily satisfied if TeV gamma rays are produced predominantly by inverse-Compton scattering with a magnetic field strength well below equipartition or by proton-synchrotron emission with a magnetic field strength near equipartition.

PACS numbers: 98.70.Rz, 98.70.Sa, 95.55.Vj

Keywords: acceleration of particles; cosmic rays; gamma ray bursts; gamma ray sources

---

\*Electronic address: fragile@llnl.gov

## I. INTRODUCTION

Evidence has been accumulating for the arrival of  $\sim$  GeV-TeV gamma rays in coincidence with low-energy ( $\sim$  MeV) gamma-ray bursts (GRBs). For example, *EGRET* detected seven GRBs which emitted high energy photons in the  $\sim$  100 MeV to 18 GeV range [1, 2, 3]. There have also been results suggestive of gamma rays beyond the GeV range [4, 5], although these were not claimed as firm detections. Evidence has also been reported for TeV emission in one burst out of 54 *BATSE* GRBs in the field of view of the *Milagro* detector [6]. In another paper Poirier et al. [7] reported suggestive evidence for sub-TeV gamma rays arriving in coincidence with GRBs which occurred near zenith above the Gamma Ray Astrophysics at Notre Dame (*GRAND*) air shower array. In that experiment, most of the eight bursts analyzed were associated with at least some marginal excess ( $\sim 1\sigma$ ) of muons including the event detected by *Milagro*. One burst evidenced a possible detection at the  $2.7\sigma$  level. As shown in Poirier et al. [7], if this detection is real, then the output in energetic gammas is likely to dominate the energetics of the burst.

Although these data are not overwhelmingly convincing, they are at least suggestive that detectable energetic TeV gamma rays might be associated with low-energy gamma-ray bursts [8]. Moreover, these new detections, if real, can not be explained by a simple extrapolation of the *BATSE* spectrum [7], particularly if intergalactic absorption is taken into account [9, 10]. A new  $\sim$  TeV component in the GRB spectrum seems to be required.

The present work is therefore an attempt to interpret these new possible detections in the context of three models, which might be proposed for the production of TeV gammas in a GRB. These are: 1) inverse-Compton scattering of ambient photons from relativistic electrons in the burst environment; 2) proton-synchrotron emission [10, 11, 12, 13]; and 3) inelastic scattering of relativistic protons from ambient photons creating high-energy neutral pions, which decay into high-energy photons [14, 15]. We here briefly outline the underlying physics and characteristic energetic gamma-ray spectra associated with each of these possible models. We then derive limits on the parameters of these models based upon the detection limits from the Project *GRAND* array. Based upon this, we conclude that it is difficult for any of these models to satisfy the energetic requirements unless the photon beaming angle is very narrow for the high-energy component. Of the models considered, the most likely are inverse-Compton scattering or proton-synchrotron emission. We note, however, that these

conclusions rely upon a few assumptions. For example, we have assumed that the low- and high-energy gamma rays are produced at the same location; that the time variability of the high-energy component can be estimated from the FWHM of the highest peak in the low-energy gamma ray light curve; and that the variability-luminosity relation of Fenimore & Ramirez-Ruiz (2000) gives a reliable estimate of the redshifts of these bursts. We explore the impact of each of these assumptions and find that, unless the bursts occur at very low redshifts ( $\lesssim 0.01$ ), the energetic requirements remain difficult to satisfy.

## II. LOW-ENERGY GRB PROPERTIES

The mystery of the astrophysical origin for low-energy gamma ray bursts (GRBs) has been with us for some time. As of yet there is no consensus explanation, although there is mounting evidence for an association with supernovae [16]. A likely scenario is a burst environment involving collisions of an ultra relativistic  $e^+ - e^-$  plasma fireball [17, 18, 19]. These fireballs may produce low-energy gamma rays either by “internal” collisions of multiple shocks [20, 21], or by “external” collisions of a single shock with ambient interstellar material [22].

In either of these paradigms it is possible for very energetic gammas to be produced through inverse-Compton scattering of ambient photons off the relativistic electrons. Furthermore, it seems likely that baryons would be accelerated along with the pair plasma to very high energies [12, 14, 23]. Synchrotron emission from energetic protons [11, 12, 13, 24] or possibly hadro-production of pions in the burst environment [15] and subsequent  $\pi^0$  gamma decay could also lead to an additional spectral component of very energetic gammas. In any case, it is at least plausible that energetic gammas could arrive in coincidence with a gamma-ray burst. This was the premise of Project *GRAND*’s search for high-energy gammas arriving in coincidence with *BATSE* GRB observations.

It is also possible, however, that low- and high-energy gamma-ray components are generated in different regions or phases of a burst. This could lead to substantially different arrival times for each component. This was in fact the case for the 18 GeV photon observed by *EGRET*, which arrived  $\sim 4500$  s after the low-energy emission had ended.

Observations of TeV gammas could provide important clues as to the baryon loading, Lorentz factor, and ambient magnetic field of the relativistic fireball. Our goal in this paper

is to constrain the possible spectrum and source of energetic photons using the Project *GRAND* data. Hence, we restrict ourselves to considering high-energy gammas produced concurrently with low-energy gammas consistent with the search technique employed by Project *GRAND*.

### III. FITS TO OBSERVED GRB SPECTRA

Table I summarizes some of the features of the *BATSE* and Project *GRAND* observations of the eight GRBs analyzed in Poirier et al. [7], where a detailed explanation of the Project *GRAND* results can be found. In the present paper, we will denote quantities in the frame of the observer by the superscript “*ob*”. We will also use  $\epsilon_\gamma$  to denote the low energy GRB photons and distinguish them from the high-energy component, denoted  $E_\gamma$ . The observed *BATSE* spectra are fit with a broken power law of the form [25]

$$\frac{d\phi_\gamma(\epsilon_\gamma^{ob})}{d\epsilon_\gamma^{ob}} = a \begin{cases} \left(\epsilon_{\gamma b}^{ob, \text{MeV}}\right)^{\beta_l - \beta_h} \left(\epsilon_\gamma^{ob, \text{MeV}}\right)^{-\beta_l}, & \text{if } \epsilon_\gamma^{ob} < \epsilon_{\gamma b}^{ob}, \\ \left(\epsilon_\gamma^{ob, \text{MeV}}\right)^{-\beta_h}, & \text{if } \epsilon_\gamma^{ob} \geq \epsilon_{\gamma b}^{ob}, \end{cases} \quad (1)$$

where  $\beta_h \approx 2$ ,  $\beta_l \approx 1$ , and  $\epsilon_{\gamma b}^{ob} \approx 1$  MeV is the break energy of the observed spectrum. Although these bursts are often better fit by using an exponential to join the two components, a broken power law is adequate for the present discussion. It maintains a simple analytic form for the equations, and as we shall see, the precise low energy form is almost irrelevant as long as a break energy exists. In what follows we will use values of  $a$ ,  $\beta_h$ ,  $\beta_l$ , and  $\epsilon_{\gamma b}^{ob}$  derived from optimum fits to the *BATSE* spectra for all events except the *Milagrito* event for which the *BATSE* fluence was too weak to obtain a reliable spectral fit. The *BATSE* fit parameters corresponding to equation (1) are listed in Table II. The fit parameters for these bursts were provided at our request by M. S. Briggs at the Marshall Space Flight Center. We also include the variability time scale  $\Delta t$  for these bursts, which was estimated as the full width at half maximum (FWHM) of the brightest peak in each light curve. The light curves of GRBs typically show a wide range of timescale variability, so this choice may not be justified. In §VII we explore the dependence of our conclusions on a wide range of values for  $\Delta t$ .

In Table III, we give estimated redshifts for each burst. GRB 990123 is the only burst in this group for which an optical counterpart was detected. This burst, therefore, is known to

have occurred at a redshift of  $z = 1.6$  [26]. The redshifts for most of the remaining bursts were estimated using the variability-luminosity relation of Fenimore & Ramirez-Ruiz [27]. This method relies on the apparent correlation between the time variability of a burst, which can be measured from its light curve, and the absolute luminosity of the burst, which we wish to infer. This provides us with a straightforward method for converting GRB observables into luminosities and redshifts [27].

Following Fenimore & Ramirez-Ruiz [27], we first fit a quadratic polynomial to the background in the non-burst portions of the *BATSE* 64 ms four channel data (i.e. DISSC data). Let  $b_i$  be the binned background counts from this polynomial fit. If  $g_i$  are the observed binned counts during the actual burst event, then the net count is  $c_i = g_i - b_i$ . We then rebin the counts by dilating the time samples by  $Y = (1 + z)/(1 + z_b)$ , where  $z$  is the redshift we wish to estimate and  $z_b$  is a baseline redshift. Following [27], we take  $z_b = 2$ . The new, dilated net counts,  $C_i$ , represent what the time history would look like at  $z = z_b$ . The variability is then defined to be the average mean-square of the variations in  $C_i$  relative to a smoothed time history, as

$$V = Y^{-0.24} \frac{1}{N} \sum \frac{(C_i - \langle C \rangle)^2 - B_i}{C_p^2}, \quad (2)$$

where  $C_p$  is the peak of the dilated net count during the burst and  $\langle C \rangle$  is the count smoothed with a square-wave window with a length equal to 15% of the duration of the burst. The  $Y^{-0.24}$  term corrects the variability for the energy-dependence of the time scale of a GRB [27]. The  $B_i$  term (dilated background counts in a sample) accounts for the Poisson noise. The sum is taken over the  $N$  samples that exceed the background by at least  $5\sigma$ . The estimated variabilities are listed in Table III.

Based upon the fits of Fenimore & Ramirez-Ruiz [27], we can relate this variability  $V$  to the peak isotropic luminosity  $L_{256}$  averaged over 256 ms in a specified energy range,  $\epsilon_{l,p}$  to  $\epsilon_{u,p}$  (i.e.  $L_{256}$  erg s $^{-1}$  in the 50 to 300 keV band). This variability-luminosity relation is

$$L_{256}/(4\pi) = 1.9 \times 10^{51} V^{0.86} \text{erg s}^{-1}. \quad (3)$$

This peak luminosity depends upon the redshift, the observed spectral shape, and the observed peak photon flux  $P_{256}$  (also averaged over 256 ms and over the same energy range) as

$$L_{256} = 4\pi D_z^2 P_{256} \langle \epsilon_\gamma \rangle, \quad (4)$$

where  $D_z$  is the co-moving distance and  $\langle \epsilon_\gamma \rangle$  is the average photon energy in the luminosity bandpass per photon in the count bandpass. For this work we compute luminosities for an isotropic burst environment, such that  $\Omega = 4\pi$ , where  $\Omega$  is the unknown opening angle of the burst. If GRBs emit in a jet, our inferred luminosities and energies are diminished by  $\Omega/4\pi$ .

The co-moving distance  $D_z$  for a flat  $\Omega_M + \Omega_\Lambda = 1$  model is simply given by

$$D_z = \frac{c}{H_0} \int_0^z [\Omega_M(1+z')^3 + \Omega_\Lambda]^{-1/2} dz' . \quad (5)$$

For the purposes of the present discussion, we will adopt the currently popular  $\Omega_M = 0.3$ ,  $\Omega_\Lambda = 0.7$ ,  $H_0 = 72 \text{ km s}^{-1} \text{ Mpc}^{-1}$  model [28, 29, 30]. From the observed photon spectrum the average photon energy in the luminosity bandpass per photon in the count bandpass is

$$\langle \epsilon_\gamma \rangle = \frac{\int_{\epsilon_l, p}^{\epsilon_u, p} \epsilon_\gamma \phi[\epsilon_\gamma/Y] d\epsilon_\gamma}{\int_{\epsilon_l}^{\epsilon_u} \phi[\epsilon_\gamma] d\epsilon_\gamma} , \quad (6)$$

where  $\epsilon_l$  and  $\epsilon_u$  are the limits on the *BATSE* energy range ( $\approx 20 - 1500 \text{ keV}$ ). We can now iteratively solve equations (2-6) until the estimate for  $z$  converges.

This method of estimating the redshift of GRBs was found [31] to be consistent with other estimates that rely upon an apparent relation between the luminosity and the time lag between hard and soft energy peaks. The correlation between these two independent methods argues in favor of their reliability [32]. However, in §VII we explore the impact of systematically larger and smaller redshifts on our conclusions.

Additionally, we can estimate the effective  $4\pi$  luminosity at the source in the *BATSE* energy band time-averaged over the full *T90* interval,  $L_\gamma$ , by

$$L_\gamma = 4\pi D_z^2 \int_{\epsilon_l}^{\epsilon_u} d\epsilon_\gamma \epsilon_\gamma \frac{d\phi[\epsilon_\gamma/(1+z)]}{d\epsilon_\gamma} . \quad (7)$$

This is the luminosity estimate we use for the rest of the work presented in this paper. Both luminosity estimates are listed in Table III for each burst.

### A. GRB 970417a

GRB 970417a was the one burst (of 54 in the field of view) for which the *Milagrito* collaboration reported evidence of TeV emission during the duration of this burst within the *BATSE* error circle [6]. For this reason, we have included it in our analysis. Interestingly,

this was a relatively weak *BATSE* burst with a fluence of  $3.9 \times 10^{-7}$  erg cm $^{-2}$  in all four *BATSE* energy channels ( $> 20$  keV). Because this is such a weak low-energy burst, it is difficult to obtain reliable fits for the *BATSE* spectral parameters. For this reason, we have instead used the following average values of all bright bursts from Preece et al. [33]:  $\beta_l = 1.0$ ,  $\beta_h = 2.25$ , and  $\epsilon_{\gamma b}^{ob} = 225$  keV. We can then use these average parameters and the observed flux to fix the normalization,  $a$ . The weak signal in the *BATSE* band also prevents us from using the variability-luminosity relation described above to determine the redshift of this burst. Instead we adopt  $z = 0.7$  based upon the analysis of Totani [10].

## IV. THE MODELS

### A. Inverse-Compton Spectrum

One possible source for energetic gamma rays is the inverse-Compton (IC) scattering of low-energy ambient photons by relativistic electrons. Indeed, such IC photons are thought to be the source of observed high-energy photons from active galactic nuclei such as Mk-421 [34].

The inverse-Compton-scattering spectrum is generally written as

$$\left(\frac{d\Phi_\gamma}{dE_\gamma}\right)_{\text{IC}} \propto E_\gamma^{-1} \int dE_e \frac{d\Phi_e}{dE_e} \int dx f_{e-s}(x) , \quad (8)$$

where  $d\Phi_e/dE_e$  is the spectrum of electrons characteristic of a Fermi mechanism,

$$\frac{d\Phi}{dE} = A \begin{cases} E^{-\alpha} , & \text{if } E < E_b, \\ E_b E^{-\alpha-1} , & \text{if } E \geq E_b, \end{cases} \quad (9)$$

where  $A$  is a normalization constant and  $\alpha \approx 2 \pm 0.2$  [35]. The flux of the synchrotron photons  $f_{e-s}$  is

$$f_{e-s}(x) = \begin{cases} x^{-(\alpha-1)/2} , & \text{below the cooling break,} \\ x^{-\alpha/2} , & \text{above the cooling break,} \end{cases} \quad (10)$$

where  $x \propto E_\gamma/E_e^2$ . Evaluating the integrals, we arrive at the simplified expression

$$(d\Phi_\gamma/dE_\gamma)_{\text{IC}} \propto E_\gamma^{-\delta} , \quad (11)$$



where the spectral index  $\delta$  is given by

$$\delta = \begin{cases} (\alpha + 1)/2, & \text{for } E_\gamma < E_{\text{cool}}, \\ (\alpha + 2)/2, & \text{for } E_\gamma > E_{\text{cool}}, \end{cases} \quad (12)$$

where  $\alpha \sim 2$  is the electron spectral index and  $E_{\text{cool}}$  is the energy scale at which the electron cooling time becomes comparable to the system lifetime. The inverse-Compton cooling time in the frame of the shock is

$$\frac{1}{t_{\text{IC}}} = 1.3 \times 10^{-4} \frac{\gamma_e L_{\gamma,51}^{\text{ob}} (1+z)^4}{\Gamma_{300}^6 \Delta t^2} \text{ s}^{-1}, \quad (13)$$

where  $\gamma_e$  is the electron Lorentz factor and  $\Gamma = 300\Gamma_{300}$  is the bulk Lorentz factor, both in the shock frame;  $L_{\gamma,51}^{\text{ob}} = L_\gamma^{\text{ob}}/10^{51} \text{ erg s}^{-1}$  where  $L_\gamma^{\text{ob}} = L_\gamma/(1+z)^2$ ; and  $\Delta t = (1+z)r_d/\Gamma^2 c$  is the variability timescale (in seconds) for the GRB, where  $r_d$  is the radius at which low-energy gamma rays are emitted, both measured in the observer frame.

The total fractional power radiated in inverse-Compton photons can be estimated from the ratio of the expansion time to the cooling time:

$$f_{\text{IC}} = \frac{\Gamma \Delta t}{(1+z)t_{\text{IC}}} \quad (14)$$

$$= 3.9 \times 10^{-2} \frac{\gamma_e L_{\gamma,51}^{\text{ob}} (1+z)^3}{\Gamma_{300}^5 \Delta t}. \quad (15)$$

The cooling frequency corresponds to  $f_{\text{IC}} = 1$ . The relation between the Compton-scattered photon energy and  $\gamma_e$  in the observer's frame is  $E_\gamma^{\text{ob}} \sim \gamma_e^2 \epsilon_\gamma^{\text{ob}}$ , where again  $\epsilon_\gamma^{\text{ob}}$  is the energy of the *BATSE* photons in the observer's frame. For simplicity we will take  $\epsilon_\gamma^{\text{ob}} = \epsilon_{\gamma b}^{\text{ob}}$ . Therefore, the cooling break energy can be written as

$$E_{\text{cool}}^{\text{ob}} = 0.66 \frac{\Gamma_{300}^{10} \Delta t^2 \epsilon_{\gamma b}^{\text{ob,MeV}}}{(L_{\gamma,51}^{\text{ob}})^2 (1+z)^6} \text{ GeV}. \quad (16)$$

Relativistic Klein-Nishina (KN) corrections to the Compton spectrum may be important in the GRB environment over some range of energies. For completeness we include these by introducing a parameter  $\Gamma_{\text{KN}} = E_\gamma^{\text{ob}} \epsilon_\gamma^{\text{ob}} (1+z)^2 / \Gamma^2 m_e^2 c^4$ . When  $\Gamma_{\text{KN}} \gg 1$ , the KN effect is important. We adopt  $\Gamma_{\text{KN}} = 1$  as the lower boundary of the KN regime. This implies a lower limit to the observed gamma energy at which the KN effects should be considered,

$$E_{\text{KN}}^{\text{ob}} \equiv 24 \frac{\Gamma_{300}^2}{(1+z)^2 \epsilon_{\gamma b}^{\text{ob,MeV}}} \text{ GeV}. \quad (17)$$

In the KN regime the emissivity of IC radiation per electron is independent of the electron energy and the cooling time becomes proportional to the electron energy [see e.g. 36]. The emissivity is reduced by a factor of  $\sim \Gamma_{\text{KN}}^{-2}$  compared with the classical IC formula (see Eq. [15]), and the observed photon energy is  $E_\gamma^{\text{ob}} \sim \Gamma \gamma_e m_e c^2 / (1+z)$ . We can thus define the cooling frequency in the KN regime, by setting  $f_{\text{IC}}^{\text{KN}} = f_{\text{IC}} \Gamma_{\text{KN}}^{-2} = 1$ . This gives

$$E_{\text{cool}}^{\text{KN},\text{ob}} = 140 \frac{L_{\gamma,51}^{\text{ob}}}{\Gamma_{300}^2 \Delta t (\epsilon_{\gamma b}^{\text{ob,MeV}})^2} \text{ GeV}, \quad (18)$$

where we have used  $E_\gamma^{\text{ob}} \sim \Gamma \gamma_e m_e c^2 / (1+z)$  for the observed Compton-scattered photon energy.

In the KN regime, the cooling is efficient in the lower photon energy range of  $E_\gamma < E_{\text{cool}}^{\text{KN}}$ , i.e., contrary to the situation in the non-KN regime. In the KN regime, the photon index becomes

$$\delta = \begin{cases} \alpha, & \text{for } E_\gamma < E_{\text{cool}}^{\text{KN}}, \\ \alpha + 1, & \text{for } E_\gamma > E_{\text{cool}}^{\text{KN}}. \end{cases} \quad (19)$$

To summarize, the IC spectrum can be modeled as

$$\left( \frac{d\Phi_\gamma}{dE_\gamma} \right)_{\text{IC}} = A_\gamma^{\text{IC}} \begin{cases} (E_\gamma^{\text{ob}})^{-(\alpha+1)/2}, & \text{if } E_\gamma < E_{\text{cool}}, \\ (E_{\text{cool}})^{1/2} (E_\gamma^{\text{ob}})^{-(\alpha+2)/2}, & \text{if } E_{\text{cool}} \leq E_\gamma < E_{\text{KN}}, \\ (E_{\text{cool}})^{1/2} (E_{\text{KN}})^{\alpha/2-1} (E_\gamma^{\text{ob}})^{-\alpha}, & \text{if } E_{\text{KN}} \leq E_\gamma < E_{\text{cool}}^{\text{KN}}, \\ (E_{\text{cool}})^{1/2} (E_{\text{KN}})^{\alpha/2-1} (E_{\text{cool}}^{\text{KN}}) (E_\gamma^{\text{ob}})^{-(\alpha+1)}, & \text{if } E_\gamma \geq E_{\text{cool}}^{\text{KN}}, \end{cases} \quad (20)$$

where all energies are assumed to be measured in GeV.

For typical parameters, all three quantities,  $E_{\text{cool}}$ ,  $E_{\text{KN}}$ , and  $E_{\text{cool}}^{\text{KN}}$  are around 1-100 GeV. In any case, the spectrum beyond  $E_\gamma \gtrsim 100$  GeV must be steep with  $\delta \sim 3$ . The resultant IC gamma-ray spectrum should cut off above

$$E_{\gamma,\text{IC}}^{\text{ob,max}} \approx E_e^{\text{ob,max}} = 4.2 \times 10^5 \frac{\Gamma_{300}^{5/2} \Delta t^{1/2}}{\xi_B^{1/4} (L_{\gamma,51}^{\text{ob}})^{1/4} (1+z)^2} \text{ GeV}, \quad (21)$$

due to the cut-off in the spectrum of ultra-relativistic electrons at energies above  $E_e^{\text{ob,max}}$ .

## B. Spectrum of Proton-Synchrotron Gamma Rays

It is generally believed that the expanding plasma contains at least some baryons. Indeed, some baryons within the jet are required to increase the burst duration and luminosity [cf.

37]. In the region where the electrons are accelerated, protons may also be accelerated up to ultra-high energies  $> 10^{20}$  eV [14] producing a spectrum characteristic of a Fermi mechanism, (eq. [9]).

The possibility of energetic protons producing  $\sim$ TeV gammas by synchrotron emission has been discussed in a number of papers [10, 11, 12, 13, 24]. This mechanism has the desirable characteristic that the low-energy photons produced by electron-synchrotron emission and the high-energy photons from energetic protons can be produced simultaneously in the same environment [12, 13].

In this model one assumes that there is a magnetic field present in the burst environment with approximate equipartition between the magnetic energy density  $B^2/8\pi$  and the total energy density,  $U$ . That is,

$$\frac{B^2}{8\pi} = \xi_B U , \quad (22)$$

where  $\xi_B$  is a fraction of order unity. Following Totani [13] we assume an optimally efficient proton-synchrotron environment in which  $U \sim U_p \sim (m_p/m_e)U_\gamma$ , where  $U_\gamma$  is the photon energy density of *BATSE* gamma rays in the frame of the burst. This latter quantity can be related to the GRB luminosity utilizing  $L_\gamma = 4\pi r_d^2 \Gamma^2 c U_\gamma$ . We can then rewrite Eq. (22) in terms of the variables introduced in the previous section. This gives

$$B = 1.4 \times 10^5 \frac{\xi_B^{1/2} (L_{\gamma,51}^{ob})^{1/2} (1+z)^2}{\Gamma_{300}^3 \Delta t} \text{ G} . \quad (23)$$

The photon energy from proton-synchrotron emission in the observer's frame is then

$$\begin{aligned} E_{\gamma,p-s}^{ob} &= \frac{\Gamma \Gamma_p^2 e \hbar B}{(1+z) m_p c} \\ &= \frac{(E_p^{ob})^2 e \hbar B (1+z)}{m_p^3 \Gamma c^5} , \end{aligned} \quad (24)$$

where  $\Gamma_p = E_p/m_p c^2$  is the relativistic gamma factor of the protons in the frame of the fireball. This leads to the desired relation between the observed proton energy and the observed gamma energy,

$$E_p^{ob} = C \times \left( E_{\gamma,p-s}^{ob, \text{GeV}} \right)^{1/2} , \quad (25)$$

where,

$$C = 1.6 \times 10^9 \frac{\Gamma_{300}^2 \Delta t^{1/2}}{\xi_B^{1/4} (L_{\gamma,51}^{ob})^{1/4} (1+z)^{3/2}} \text{ GeV} . \quad (26)$$

The final quantity needed to derive the energetic gamma spectrum is the cooling rate due to synchrotron emission. In the frame of the shock, the synchrotron cooling rate is

$$\begin{aligned} \frac{1}{t_{p\text{-sync}}} &\equiv -\frac{1}{E_p} \frac{dE_p}{dt} \\ &= \frac{4e^4 B^2 E_p^{ob}(1+z)}{9m_p^4 c^7 \Gamma} \\ &= 7.5 \times 10^{-2} \frac{\xi_B^{3/4} (L_{\gamma,51}^{ob})^{3/4} (1+z)^{7/2}}{\Gamma_{300}^5 \Delta t^{3/2}} (E_\gamma^{ob, \text{GeV}})^{1/2} \text{ s}^{-1}. \end{aligned} \quad (27)$$

The fractional energy loss to synchrotron photons then becomes

$$\begin{aligned} f_{p\text{-sync}}(E_p^{ob}) &\simeq \frac{\Gamma \Delta t}{(1+z)t_{p\text{-sync}}} \\ &= \begin{cases} \frac{E_p^{ob}}{E_{pb,p-s}^{ob}}, & \text{if } E_p^{ob} < E_{pb,p-s}^{ob}, \\ 1, & \text{if } E_p^{ob} \geq E_{pb,p-s}^{ob}, \end{cases} \end{aligned} \quad (28)$$

where

$$E_{pb,p-s}^{ob} = 7.5 \times 10^7 \frac{\Gamma_{300}^6 \Delta t}{\xi_B L_{\gamma,51}^{ob} (1+z)^4} \text{ GeV}. \quad (29)$$

Finally, we note that a proton flux  $\Phi_p(E_p)$  will produce an energetic gamma flux of

$$\Phi_\gamma = \frac{E_p}{E_\gamma} f_\pi(E_p) \Phi_p. \quad (30)$$

The observed high-energy photon spectrum can then be derived from equations (9), (30), and (25),

$$\frac{d\Phi_\gamma}{dE_\gamma} = \frac{d\Phi_p}{dE_p} \times \frac{dE_p}{dE_\gamma} \times \frac{d\Phi_\gamma}{d\Phi_p}, \quad (31)$$

to yield

$$\left( \frac{d\Phi_\gamma}{dE_\gamma} \right)_{p-s} = \frac{1}{2} A_p^{\text{p-sync}} C^{2-\alpha} \times \begin{cases} \left( E_{\gamma b,p-s}^{ob, \text{GeV}} \right)^{-1/2} \left( E_\gamma^{ob, \text{GeV}} \right)^{-(\alpha+1)/2}, & \text{if } E_\gamma^{ob} < E_{\gamma b,p-s}^{ob}, \\ \left( E_\gamma^{ob, \text{GeV}} \right)^{-(\alpha+2)/2}, & \text{if } E_\gamma^{ob} \geq E_{\gamma b,p-s}^{ob}, \end{cases} \quad (32)$$

where  $A_p^{\text{p-sync}}$  is a normalization constant to be determined from observations. The break energy is

$$E_{\gamma b,p-s}^{ob} = 2.1 \times 10^{-3} \frac{\Gamma_{300}^8 \Delta t}{\xi_B^{3/2} (L_{\gamma,51}^{ob})^{3/2} (1+z)^5} \text{ GeV}. \quad (33)$$

The gamma-ray spectrum should cut off above  $E_{\gamma,p-s}^{ob, \text{max}} \approx 15\Gamma_{300}/(1+z)$  TeV [13] due to the cut-off in the spectrum of ultra-relativistic protons at energies above

$$E_p^{ob, \text{max}} = 2.1 \times 10^{11} \frac{\Gamma_{300}^{5/2} \Delta t^{1/2}}{\xi_B^{1/4} (L_{\gamma,51}^{ob})^{1/4} (1+z)^2} \text{ GeV}. \quad (34)$$

### C. Spectrum of Photo-Pion Gamma Rays

Along with undergoing synchrotron radiation, protons accelerated in the burst environment may collide with photons in the expanding fireball to produce secondary pions, which subsequently decay into high-energy gammas and neutrinos. This source of gamma rays seems unlikely due to the fact that it results from a secondary strong interaction and therefore has a small cross-section relative to electromagnetic interactions. Nevertheless an estimate of this spectrum is straightforward, so we include it here. Another alternative possibility might be pion production via proton-proton collisions [cf. 20]. However, the proton density in the frame of the shock must be small to ensure a low optical depth for gammas. Hence,  $p-\gamma$  collisions are favored over  $p-p$ , although as we will show, even this preferred reaction places unreasonable energetic requirements on the burst environment.

Following Waxman & Bahcall [15], the energy loss rate due to pion production is

$$\frac{1}{t_\pi} = \frac{1}{2\Gamma_p^2} \int_{E_0}^{\infty} dE \sigma_\pi(E) \xi(E) E \int_{E/2\Gamma_p}^{\infty} \frac{d\epsilon}{\epsilon^2} \frac{d\phi_\gamma(\epsilon)}{d\epsilon}, \quad (35)$$

where  $E_0 \approx 0.15$  GeV is the threshold for pion production. In the first integral,  $\sigma_\pi$  is the cross section for pion production due to a collision with a photon of energy  $\epsilon_\gamma$  in the rest frame of the proton, and  $\xi(E)$  is the average fractional energy lost to the pion. The second integral is over the low energy GRB spectrum, where  $\phi_\gamma(\epsilon_\gamma)$  is the photon flux in the frame of the proton.

The evaluation of  $t_\pi$  can be simplified [15] by integrating the pion production cross section over the broken-power-law GRB spectrum (Eq. [1]) transformed back to the frame of the expanding plasma. Approximating the integral over the pion production cross section by the contribution from the peak of the  $\Delta$ -resonance [as in 15] we deduce  $t_\pi$  for a general spectral power law index  $\beta_i$ :

$$\frac{1}{t_\pi} = \frac{cU_\gamma}{\epsilon_{\gamma b}} \frac{\sigma_{peak} \xi_{peak}}{(1 + \beta_i)} \frac{\Delta E_{peak}}{E_{peak}} \times \min \left[ 1, \left( \frac{2\Gamma_p \epsilon_{\gamma b}}{E_{peak}} \right)^{\beta_i - 1} \right] \text{ s}^{-1}, \quad (36)$$

where  $\sigma_{peak} \approx 5 \times 10^{-28}$  cm<sup>2</sup> is the  $\Delta$ -resonance cross section, while  $E_{peak} = 0.3$  GeV and  $\Delta E_{peak} \simeq 0.2$  GeV are the energy and width of the resonance, respectively. The fractional energy lost at the peak is  $\xi_{peak} \approx 0.2$ , and  $U_\gamma$  is the photon energy density of *BATSE* gamma rays in the frame of the fireball, as before.

As before we estimate the fractional power radiated as

$$\begin{aligned}
f_\pi &= \frac{\Gamma \Delta t}{(1+z)t_\pi} \\
&= \frac{4.5 \times 10^{-4} L_{\gamma,51}^{ob} (1+z)^2}{(1+\beta_i) \epsilon_{\gamma b}^{ob, \text{MeV}} \Gamma_{300}^4 \Delta t} \begin{cases} \times \left( \frac{E_p^{ob}}{E_{pb,\pi}^{ob}} \right)^{\beta_h - 1}, & \text{if } E_p^{ob} < E_{pb,\pi}^{ob}, \\ \times 1, & \text{if } E_p^{ob} \geq E_{pb,\pi}^{ob}, \end{cases} \quad (37)
\end{aligned}$$

where  $\epsilon_{\gamma b}^{ob} \approx 1$  MeV is the break energy of the two power laws of the observed GRB spectrum. The last factor in equation (37) describes a break in the proton spectrum. In the observer frame this break energy is [15]

$$E_{pb,\pi}^{ob} = 1.3 \times 10^7 \frac{\Gamma_{300}^2}{(1+z)^2 \epsilon_{\gamma b}^{ob, \text{MeV}}} \text{ GeV} . \quad (38)$$

Roughly half of the energy lost by the protons goes into  $\pi^+$ 's, which quickly decay into neutrinos and positrons (through  $\mu^+$ s). In this work, we have ignored the effects of these decay products on the emerging gamma-ray spectrum. For neutrinos this is reasonable since there is very little chance of them interacting further. The positrons, however, may influence the gamma-ray spectrum through positron-synchrotron radiation [24] or pair annihilation.

The other half of the energy lost by the protons goes into  $\pi^0$ 's, which then decay into two photons. The mean pion energy is  $\xi_{peak} E_p$ . When the  $\pi^0$  decays, the energy is shared equally among the photons. Hence, each gamma ray has an average energy

$$E_\gamma = \xi_{peak} E_p / 2 . \quad (39)$$

Now from equation (31)

$$\begin{aligned}
\left( \frac{d\Phi_\gamma}{dE_\gamma} \right)_\pi &= f_\pi \left( \frac{2}{\xi_{peak}} \right)^{2-\alpha} A E_\gamma^{-\alpha} \\
&= A_p^\pi D_\pi \times \begin{cases} (1+\beta_h)^{-1} \left( E_{\gamma b,\pi}^{ob, \text{GeV}} \right)^{1-\beta_h} \left( E_\gamma^{ob, \text{GeV}} \right)^{\beta_h - \alpha - 1}, & \text{if } E_\gamma^{ob} < E_{\gamma b,\pi}^{ob}, \\ (1+\beta_l)^{-1} \left( E_\gamma^{ob, \text{GeV}} \right)^{-\alpha}, & \text{if } E_\gamma^{ob} \geq E_{\gamma b,\pi}^{ob}, \end{cases} \quad (40)
\end{aligned}$$

where  $A_p^\pi$  is a normalization constant and

$$D_\pi = 4.5 \times 10^{-4} \frac{L_{\gamma,51}^{ob} (1+z)^{2-\alpha}}{\epsilon_{\gamma b}^{ob, \text{MeV}} \Gamma_{300}^4 \Delta t} \left( \frac{2}{\xi_{peak}} \right)^{2-\alpha} . \quad (41)$$

The observed break energy  $E_{\gamma b,\pi}^{ob}$  in the pion decay gamma spectrum is given by

$$E_{\gamma b,\pi}^{ob} = \frac{\xi_{peak}}{2} E_{pb,\pi}^{ob} \approx 1.3 \times 10^6 \frac{\Gamma_{300}^2}{(1+z)^2 \epsilon_{\gamma b}^{ob, \text{MeV}}} \text{ GeV} . \quad (42)$$

Above this energy the spectrum should obey the  $d\Phi_\gamma/dE_\gamma \sim E_\gamma^{-2}$  of the protons and below this break energy, the exponent should be harder by one power, i.e.  $d\Phi_\gamma/dE_\gamma \sim E_\gamma^{-1}$ . As a practical matter, photons with energy as high as the break energy will not be observed, as they will be extinguished by pair production as described below.

## V. PHOTON, PROTON, AND ELECTRON LUMINOSITIES AT THE SOURCE

From the above it is clear that the three models considered here imply different spectral shapes for the high-energy gamma component. Figure 1 compares the initial spectra for all three mechanisms normalized to reproduce the Project *GRAND* observations for GRB 971110 (as explained in Section 7). This would correspond to the unrealistic limit of no self or intergalactic absorption. Nevertheless, this illustrates the fact that these mechanisms have significantly different energetic requirements. Clearly, the most favorable energetically are the inverse-Compton and proton-synchrotron models. Figure 2 further illustrates this point by reproducing the source proton and electron spectra required by the various models, again normalized to reproduce the Project *GRAND* observations. Also included in this figure is the source electron spectrum required to only produce the observed *BATSE* data for this burst, following the electron-synchrotron model. The Project *GRAND* result, if it represents a real detection, requires a much higher flux of electrons to produce sufficient high-energy gamma rays through inverse-Compton scattering. This is probably a troubling requirement for the inverse-Compton model.

To calculate these spectra we have used the normalization of the gamma-ray spectrum from the observed muon excess to determine the normalization of the associated ultra-relativistic proton and electron spectra. This is straightforward for the proton-synchrotron and photo-pion models, since the proton normalization appears explicitly in our final expressions (equations [40] and [32]). For the inverse-Compton model, we have followed Sari & Esin [38] to estimate the electron normalization from the following approximate relation between the low-energy electron-synchrotron spectrum, assumed to be observed by *BATSE*, and the inverse-Compton spectrum in the energy range of Project *GRAND*

$$E_\gamma \left( \frac{d\Phi_\gamma}{dE_\gamma} \right)_{\text{IC}} \simeq 0.5 r_d \sigma_T n \epsilon_\gamma \left( \frac{d\phi_\gamma}{d\epsilon_\gamma} \right)_{\text{e-s}} . \quad (43)$$

We take the electron number density  $n$  to be  $1 \text{ cm}^{-3}$ . The electron-synchrotron spectrum

is assumed to have a form directly comparable to equation (32). We evaluate equation (43) at  $E_\gamma = E_{\text{cool}}^{\text{ob}}$  and  $\epsilon_\gamma = \epsilon_{\gamma b}^{\text{ob}}$  to find  $A_e^{\text{e-sync}}$ .

On the other hand, if one attributes [14] the observed cosmic-ray excess above  $10^{20}$  eV to the energetic protons accelerated in GRBs, then an independent estimate of the proton normalization at the source can be obtained. Following Waxman [14] we note that the observed cosmic ray flux above  $10^{20}$  eV is  $\sim 3 \times 10^{-21} \text{ cm}^{-2} \text{ s}^{-1} \text{ sr}^{-1}$  [39], corresponding to an average universal number density of energetic cosmic rays of  $n_{CR} \sim 10^{-30} \text{ cm}^{-3}$ . If this density is due to GRBs then the number of protons with energies greater than  $10^{20}$  eV produced per GRB must be

$$N(E_p > 10^{20}) = n_{CR}/\nu_\gamma\tau_{CR} \sim 5 \times 10^{44} \quad , \quad (44)$$

where  $\nu_\gamma \approx 2 \times 10^{-10}(h/70)^3 \text{ Mpc}^{-3} \text{ yr}^{-1}$  is the cosmological GRB rate [40, 41, 42], and  $\tau_{CR} \approx 3 \times 10^8 \text{ yr}$  is the lifetime of protons with  $E_p > 10^{20}$  eV. With our nominal  $E_p^{-2}$  spectral form, we deduce an absolute normalization of the proton spectrum emerging from an average GRB source of  $dN_p/dE_p = 5 \times 10^{55} E_{\text{GeV}}^{-2} \text{ GeV}^{-1}$ . This is to be compared with the number of photons with  $E > 1 \text{ MeV}$  emerging from a nominal GRB. If we assume that  $10^{53} \text{ erg}$  is released in gammas above 1 MeV for an energetic photon spectrum of  $d\Phi_\gamma/dE_\gamma \propto E_\gamma^{-2}$ , then the normalized spectrum for gammas above 1 MeV would be  $dN_\gamma/dE_\gamma = 6 \times 10^{58} E_{\text{GeV}}^{-2} \text{ GeV}^{-1}$ . Thus, one expects about 1200 gammas per proton from such a burst.

Since both the proton-synchrotron and photo-pion models are based upon the same underlying baryon content in the relativistic plasma, it is instructive to summarize the relative efficiency of these two mechanisms for generating energetic gamma rays in GRBs. Let us consider a typical burst with  $\beta_h = 2$  and a proton spectrum with  $\alpha = 2$ . Then in the region  $E_\gamma^{\text{ob}} \sim 1 \text{ TeV}$ , the fractional energy loss into these two mechanisms is

$$f_\pi = 1.7 \times 10^{-7} \frac{L_{\gamma,51}^{\text{ob}}(1+z)^4}{\Gamma_{300}^6 \Delta t} \left( \frac{E_\gamma^{\text{ob}}}{\text{TeV}} \right) \quad , \quad (45)$$

and

$$f_{\text{p-sync}} = \min \left\{ 1, \left[ 6.7 \times 10^2 \frac{\xi_B^{3/4} (L_{\gamma,51}^{\text{ob}})^{3/4} (1+z)^{5/2}}{\Gamma_{300}^4 \Delta t^{1/2}} \left( \frac{E_\gamma^{\text{ob}}}{\text{TeV}} \right)^{1/2} \right] \right\} \quad . \quad (46)$$

The factor of  $1.7 \times 10^{-7}$  suggests that proton-synchrotron emission will dominate over the photo-pion production for the parameters and gamma-ray energy considered. Only for



sufficiently small  $\xi_B$  ( $\lesssim 10^{-4}$ ) does the efficiency of the proton-synchrotron mechanism begin to deviate from unity as  $\xi_B^{3/4}$ .

A direct comparison between inverse-Compton scattering and proton-synchrotron emission is not possible since these two mechanisms rely upon different underlying energy sources, i.e. relativistic electrons for inverse-Compton scattering and relativistic protons for proton-synchrotron emission. Nevertheless, we note that both of these methods can be very efficient. In the region  $E_\gamma^{ob} \sim 1$  TeV,  $f_{IC} \sim 1$  and  $f_{p\text{-sync}} \sim 1$  for the range of parameters considered. This suggests that inverse-Compton scattering provides a very competitive mechanism for the generation of energetic gammas. Furthermore, it makes no requirement on the pre-existence of a magnetic field or baryon loading in the fireball plasma.

Another important difference among all of these mechanisms is their associated cut-off energies. As noted above, there should be a cut-off for the proton-synchrotron spectrum around  $E_{\gamma,p-s}^{ob,max} \approx 15$  TeV, corresponding to a cut-off in the ultra-relativistic proton energies. The inverse-Compton spectrum has a much larger cut-off at around  $E_{\gamma,IC}^{ob,max} \approx 400$  TeV, corresponding to a cut-off in the relativistic electron energies. For pion decay, however, the spectrum may extend all the way to  $10^7$  TeV [15], but with a break at around 1300 TeV. These differences have a large effect on the implied total source luminosities of the bursts, as is apparent in Figure 1.

## VI. PAIR PRODUCTION OPTICAL DEPTH

The spectra derived above must be corrected for two effects, both of which are due to pair production by energetic photons. First, within the burst environment, energetic gamma rays will interact with other photons to produce  $e^+ - e^-$  pairs. If this process is highly efficient,  $\sim$  TeV gamma rays may not be able to escape from the burst. Even if some photons escape, this self-absorption will affect the implied source luminosity.

The second effect is due to absorption along the line-of-sight from the burst environment. Here the energetic gamma rays interact with the intergalactic infrared and microwave backgrounds. This effect can cause a dramatic shift in the spectrum of energetic gammas in the TeV range depending upon the distance to the burst.

### A. Internal Optical Depth from Pair Production

A photon of energy  $E_\gamma$  interacts mainly with target photons of energy  $\epsilon_\gamma \sim 2m_e^2 c^4 / E_\gamma$  in the shock frame. We can approximate the cross section for pair-production as  $3\sigma_T/16$ , where  $\sigma_T = 6.6 \times 10^{-25} \text{ cm}^2$  is the Thomson cross section. Then the optical depth can be approximated as

$$\tau_{\gamma\gamma,int} \sim \frac{3}{16} \sigma_T \frac{D_z^2}{r_d^2} \epsilon_\gamma \frac{d\phi_\gamma[\epsilon_\gamma/(1+z)]}{d\epsilon_\gamma} \frac{\Delta t}{\Gamma(1+z)}, \quad (47)$$

where  $\Delta t\Gamma/(1+z)$  is the width of the emitting region as measured in the shock frame.

This formula is similar to that of Waxman & Bahcall [15], except that this form takes into account the spectral break in the low-energy GRB photons. This break is important since it implies that the optical depth is proportional to  $\sim E_\gamma$  for  $E_\gamma^{ob} \lesssim 2m_e^2 c^4 \Gamma^2 / \epsilon_{\gamma b}^{ob} \approx 50 \text{ GeV}$ , but roughly constant for higher energies. The Waxman & Bahcall [15] result is only valid in the lower energy range. The proper energy dependence is important because the internal optical depth can be of order unity. In the case of GRB 971110, the internal optical depth at 100 GeV is  $\approx 3$  implying that some energetic gammas could emerge. The thin lines in Figure 1 show how the three source spectra normalized to fit GRB 971110 would be modified by internal absorption. The change in the energy dependence of the internal optical depth is apparent above about 50 GeV. For the remainder of the bursts, we were unable to place meaningful constraints on the internal optical depth due to large uncertainties in the fit parameters, particularly  $\beta_h$  and  $\Gamma$ . For these bursts, we have taken the very optimistic assumption of  $\tau_{\gamma\gamma,int} = 0$ .

### B. Intergalactic Optical Depth from Pair Production

Another important constraint on the observed burst spectra comes from the absorption of photons via pair production during collisions with the intergalactic infrared background. In this work we use a calculated optical depth for intergalactic absorption based upon the standard formulation [e.g. 9]. We use a model for the luminosity evolution of background light from Totani, Yoshii, & Sato [43]. The dust emission component is calculated assuming a dust emission spectrum similar to that of the Solar neighborhood. The fraction of light absorbed by dust is adjusted to reproduce the observed far infrared background from COBE [44]. This method is summarized in Totani [10]. It is consistent with other optical-depth

calculations [cf. 9, 45].

The resultant  $e^+ - e^-$  pairs may then further modify the original gamma-ray spectrum by providing a medium for some of the remaining gamma rays to undergo intergalactic inverse-Compton scattering. This process results in complicated showers of secondary electrons and gammas. These secondary gammas may be observed, but over a much longer time-scale, since much of this secondary light traverses a longer path length. The flux from these secondary gamma rays is probably below the detection threshold of current arrays such as Project *GRAND*. Nevertheless, this might be a noteworthy effect.

Figure 3 shows final spectra in the observer’s frame when both internal and intergalactic absorption are taken into account, assuming the burst is arriving from a redshift of  $z = 0.6$  (appropriate for GRB 971110). Even though the source spectra are vastly different, the observed high-energy gamma spectra are quite similar. Hence, the implied source energy requirement may be the only way to distinguish between the models. For illustration, Figure 3 also includes the observed *BATSE* spectrum for this burst, fit with both the Band (Eq. [1]) and electron-synchrotron models.

## VII. RESULTS

In this work we use the muon observations of Project *GRAND* to fix the normalization (or upper limit) in each of the models described above for the various bursts analyzed. That is, the spectral shape is fixed from equations (40), (32), or (20), and the number of muons expected is then computed using

$$N_\mu = dA \times T90 \times \int_{E_{min}}^{\infty} dE_\gamma^{ob} P_\mu(E_\gamma^{ob}) \frac{d\Phi_\gamma(E_\gamma^{ob})}{dE_\gamma^{ob}} \exp(-\tau_{\gamma\gamma}) , \quad (48)$$

where  $dA$  is the collecting area of the Project *GRAND* array (the effective area at the time of GRB 971110 was approximately  $6.3 \times 10^5$  cm<sup>2</sup>),  $E_{min}$  is the primary gamma-ray detection threshold for Project *GRAND* ( $\sim 10$  GeV), and  $P_\mu \approx 7.0 \times 10^{-5} (E_\gamma^{\text{GeV}})^{1.17}$  is the probability per primary for a muon to reach detection level at Project *GRAND*. This probability (valid for  $E_\gamma \gtrsim 3$  GeV) was computed by Fasso & Poirier [46] using the Monte Carlo atmospheric absorption code, *FLUKA*. Here  $\tau_{\gamma\gamma}$  includes both the internal and intergalactic optical depth estimated for each burst as described above. For illustration, Table IV summarizes some estimates of the relative magnitudes of internal and intergalactic optical depths at two energy

scales, 100 GeV and 1 TeV.

In practice, the integral in equation (48) is cut off at  $\approx 30$  TeV since the optical depth is quite high for photons above this energy. The normalization constants for each model are then adjusted so that  $N_\mu$  agrees with the  $2\sigma$  upper limits set by Project *GRAND*, except for GRB 971110 where we used the observed mean value (see Table I). Here we adopt typical values for the degree of equipartition  $\xi_B$  and the relativistic Lorentz factor  $\Gamma$ , namely  $\xi_B \approx 1$  and  $\Gamma \approx 300$ . Below we explore the dependence of our results on a broad range of these parameters.

We can then use our normalized gamma spectra to estimate the total energy emitted in high-energy gammas at the source. For the inverse-Compton model, we can also estimate the energy emitted in electrons, noting again the characteristic spectrum of a Fermi mechanism given in equation (9). Similarly we can estimate the energy emitted in protons for the proton-synchrotron and photo-pion models. Implied energies for photon emission into  $4\pi$  are given in Tables V, VI, and VII for the inverse-Compton, proton-synchrotron, and photo-pion models, respectively. We also list the required energies of the source protons or electrons, as appropriate. Our results assume  $\alpha = 2$  for the accelerated electron and proton spectra. For GRB 971110 we estimated the statistical uncertainties of our results using Monte Carlo techniques to explore the parameter space of each of the models assuming Gaussian error distributions.

As evidenced by the large uncertainties, the models are not well constrained at present. Nevertheless, several points are worth noting from the tables. For the most significant possible detection (GRB 971110), the energetic requirements for the IC model ( $E_\gamma^{Tot,IC} = (2.6 \pm 8.6) \times 10^{55}$  erg) and the proton-synchrotron model ( $E_\gamma^{Tot,p-sync} = (3. \pm 10.) \times 10^{55}$  erg) are much less than that for a photo-pion mechanism ( $E_\gamma^{Tot,\pi} = (4. \pm 27.) \times 10^{62}$  erg), as expected.

The distinction between the inverse-Compton and proton-synchrotron mechanisms has an important consequence on the magnetic field of the GRB, specifically the degree of equipartition,  $\xi_B$ . In the case of inverse-Compton scattering, the ratio of the inverse-Compton luminosity  $L_\gamma^{IC}$  to electron-synchrotron luminosity  $L_{sync}$  should be equal to the ratio of the IC target photon energy density  $U_\gamma$  to the magnetic field energy density  $U_B$  since both

mechanisms arise from the same population of hot relativistic electrons. Thus,

$$\frac{L_\gamma^{\text{IC}}}{L_{\text{sync}}} = \frac{U_\gamma}{U_B}, \quad (49)$$

where  $U_B = \xi_B U$  and  $U$  is the total rest-frame energy density of the emission region. If we adopt the generally accepted view that the  $\sim$ MeV gamma rays seen by *BATSE* are caused by electron-synchrotron radiation then  $L_{\text{sync}} = L_\gamma$ . For GRB 971110,  $L_\gamma^{\text{IC}}/L_\gamma \sim 10^4$ , which implies

$$\xi_B U \lesssim 10^{-4} U_\gamma. \quad (50)$$

Since the energy density of the  $\sim$ MeV *BATSE* gamma rays is likely to be higher than any other radiation source available for inverse-Compton scattering, we identify this energy density as  $U_\gamma$ . This association has been implicit throughout this paper. On the other hand, since  $L_\gamma^{\text{IC}} \sim 10^4 L_\gamma$  the energy density of the  $\sim$ TeV gamma rays must be greater than  $U_\gamma$  by about  $10^4$ . We can then use  $10^4 U_\gamma$  as a lower limit for the total rest-frame energy density  $U$ . Combining this with Eq. (50) we get the following upper limit on the degree of equipartition

$$\xi_B \lesssim 10^{-8}. \quad (51)$$

Note also that Eq. (49) holds only in the classical regime. In the KN regime  $\xi_B$  is even smaller because inverse-Compton scattering becomes less efficient. Hence, the inverse-Compton model is at odds with models that propose GRBs as the source of ultra-high energy cosmic rays, since those models require a magnetic field near equipartition,  $\xi_B \sim 1$  [cf. 14].

In Figures 4, 5, and 6 we explore the dependence of our results upon a broad range of possible values for  $\Gamma$ ,  $\xi_B$ , and  $\Delta t$ , respectively. These uncertainties were not formally included in our statistical estimates. Nevertheless, these figures support our qualitative conclusions. Specifically, the energetic requirements of all three models are in excess of that for the GRB for a broad range of parameters. Indeed most parameter variations in Figures 4 - 6 only exacerbate this problem. However, the inverse-Compton and proton-synchrotron mechanisms are generally less sensitive to changes in  $\Gamma$  over the range  $100 \lesssim \Gamma \lesssim 1000$  or changes in  $\Delta t$  over the range  $0.1 \lesssim \Delta t \lesssim 10$ . The sharp increase in the energy content of the protons and electrons at small  $\Gamma$  enters primarily through the internal optical depth. Figure 5 shows that the proton-synchrotron mechanism is highly efficient over a fairly broad range of  $\xi_B$  ( $\gtrsim 0.01$ ).

Regardless of the mechanism, if GRB 971110 is indeed a detection and our estimated redshift of  $z = 0.6$  is valid, the implied energy in energetic ( $E_\gamma > 1$  GeV) gamma rays is more than 100 times higher than the energy in the low-energy gamma rays. This renders the already challenging energetic requirements on the GRB source engine to be even more difficult. It may be possible to alleviate this difficulty if, perhaps, the photon beaming angle is much narrower for the high-energy component than for the low-energy GRB. Another possibility is that the redshift is much lower than our estimated value for this burst. In Figure 7 we explore the energetic requirements for GRB 971110 over a very broad range of redshifts from 0.005 to 3. This range is consistent with most currently measured GRB redshifts. This figure illustrates quite clearly the critical role that intergalactic absorption plays in driving up the energetic requirements and highlights the need for accurately determining the true redshifts of GRBs.

## VIII. CONCLUSION

We have analyzed the eight GRBs discussed in Poirier et al. [7], which occurred above the Project *GRAND* array. We have studied the implied energies in energetic ( $\sim$ TeV) gamma rays (and associated electrons and protons) of such GRBs in the context of three possible mechanisms: inverse-Compton scattering, proton-synchrotron radiation, and photo-pion production. Our analysis suggest that all of these models face significant energetic requirements. Gamma-ray production by either inverse-Compton scattering or proton-synchrotron radiation is probably the most efficient process.

Although it can not be claimed that TeV gammas have unambiguously been detected in association with low-energy GRBs, we have argued that there is enough mounting evidence to warrant further study. Furthermore, we have shown that if TeV gammas continue to be observed, then they present some interesting dilemmas for GRB physics. In view of their potential as a probe of the GRB source environment, we argue that further efforts to measure energetic gamma rays in association with low-energy gamma-ray bursts are warranted.

## Acknowledgments

The authors would like to thank M. S. Briggs for providing fits to these *BATSE* data. This research has made use of data obtained from the High Energy Astrophysics Science Archive Research Center, provided by NASA's Goddard Space Flight Center. Project *GRAND*'s research is presently being funded through a grant from the University of Notre Dame and private grants. This work was supported in part by DoE Nuclear Theory grant DE-FG02-95ER40934 at the University of Notre Dame. This work was performed in part under the auspices of the US Department of Energy by the University of California, Lawrence Livermore National Laboratory under contract W-7405-Eng-48. One of the authors (TT) wishes to acknowledge support under a fellowship for research abroad provided by the Japanese Society for the Promotion of Science.

- 
- [1] Schneid, E. J., et al. 1992, *Astron. Astrophys.*, 255, L13
- [2] Hurley, K. 1994, *Nature*, 372, 652
- [3] Catelli, J. R., Dingus, B. L. & Schneid, E. J. 1997, in *Gamma Ray Bursts*, ed. C. A. Meegan (New York: AIP)
- [4] Amenomori, M., et al. 1996, *Astron. Astrophys.*, 311, 919
- [5] Padilla, L., et al. 1998, *Astron. Astrophys.*, 337, 43
- [6] Atkins, R., et al. 2000, *Astrophys. J.*, 533, L119
- [7] Poirier, J., D'Andrea, C., Fragile, P. C., Gress, J., Mathews, G. J., Race, D. 2003, *Phys. Rev. D*, 67, 042001
- [8] Vernetto, S. 2000, *Astropart. Phys.*, 13, 75
- [9] Salamon, M. H. & Stecker, F. W. 1998, *Astrophys. J.*, 493, 547
- [10] Totani, T. 2000, *Astrophys. J.*, 536, L23
- [11] Vietri, M. 1997, *Phys. Rev. Lett.*, 78, 4328
- [12] Totani, T. 1998a, *Astrophys. J.*, 502, L13
- [13] Totani, T. 1998b, *Astrophys. J.*, 509, L81
- [14] Waxman, E. 1995, *Phys. Rev. Lett.*, 75, 386
- [15] Waxman, E. & Bahcall, J. 1997, *Phys. Rev. Lett.*, 78, 2292
- [16] Garnavich, P., et al. 2002, *BAS*, 200, 2505
- [17] Paczyński, B. 1986, *Astrophys. J.*, 308, L43
- [18] Goodman, J. 1986, *Astrophys. J.*, 308, L47
- [19] Sari, R., Piran, T., & Narayan, R. 1998, *Astrophys. J.*, 497, L17
- [20] Paczyński, B. & Xu, G. 1994, *Astrophys. J.*, 427, 708
- [21] Mészáros, P. & Rees, M. J. 1994, *Mon. Not. R. Astron. Soc.*, 269, L41
- [22] Rees, M. & Mészáros, P. 1992, *Mon. Not. R. Astron. Soc.*, 258, P41
- [23] Vietri, M. 1995, *Astrophys. J.*, 453, 883
- [24] Böttcher M. & Dermer, C. D. 1998, *Astrophys. J.*, 499, L131
- [25] Band, D. et al. 1993, *Astrophys. J.* 413, 281
- [26] Kulkarni, S. R., et al. 1999, *Nature*, 398, 389
- [27] Fenimore, E. E. & Ramirez-Ruiz, E. 2000, preprint(astro-ph/0004176) [Our analysis is based



upon an early preprint of this paper. In later revisions the authors somewhat altered their equations from what is used in this work. Nevertheless, the earlier version is adequate for our purposes.]

- [28] Garnavich, P. M., et al. 1998, *Astrophys. J.*, 493, L53
- [29] Perlmutter, S., et al. 1998, *Nature*, 391, 51
- [30] Freedman, W. L., et al. 2001, *Astrophys. J.*, 553, 47
- [31] Reichart, D. E., Lamb, D. Q., Fenimore, E. E., Ramirez-Ruiz, E., Cline, T. L., & Hurley, K. 2001, *Astrophys. J.*, 522, 57
- [32] Schaefer, B. E., Deng, M. & Band, D. L. 2001, *Astrophys. J.*, 563, L123
- [33] Preece, R. D., Briggs, M. S., Mallozzi, R. S., Pendleton, G. N., Paciesas, W. S., & Band, D. L. 2000, *Astrophys. J. Supp.*, 126, 19
- [34] Zdziarski, A. A. & Krolik, J. H. 1993, *Astrophys. J.*, 409, L33
- [35] Hillas, A. M. 1984, *ARA&A*, 22, 425
- [36] Brumenthal, G. R. & Gould, R. J. 1970, *Rev. Mod. Phys.*, 42, 237
- [37] Salmonson, J., Wilson, J. R. & Mathews, G. J. 2001, *Astrophys. J.*, 553, 471
- [38] Sari, R. & Esin, A. A. 2001, *Astrophys. J.*, 548, 787
- [39] Bird, D. J., et al. 1994, *Astrophys. J.*, 424, 491
- [40] Totani, T. 1997, *Astrophys. J.*, 486, L71
- [41] Totani, T. 1999, *Astrophys. J.*, 511, 41
- [42] Schmidt, M. 1999, *Astrophys. J.*, 523, L117
- [43] Totani, T., Yoshii, Y., & Sato, K. 1997, *Astrophys. J.*, 483, L75
- [44] Hauser, M. G., et al. 1998, *Astrophys. J.*, 508, 25
- [45] Primack, J. R., Bullock, J. S., Somerville, R. S., & MacMinn, D. 1999, *Astropart. Phys.*, 11, 93
- [46] Fasso, A. & Poirier, J. 2001, *Phys. Rev. D*, 63, 036002 (2001)

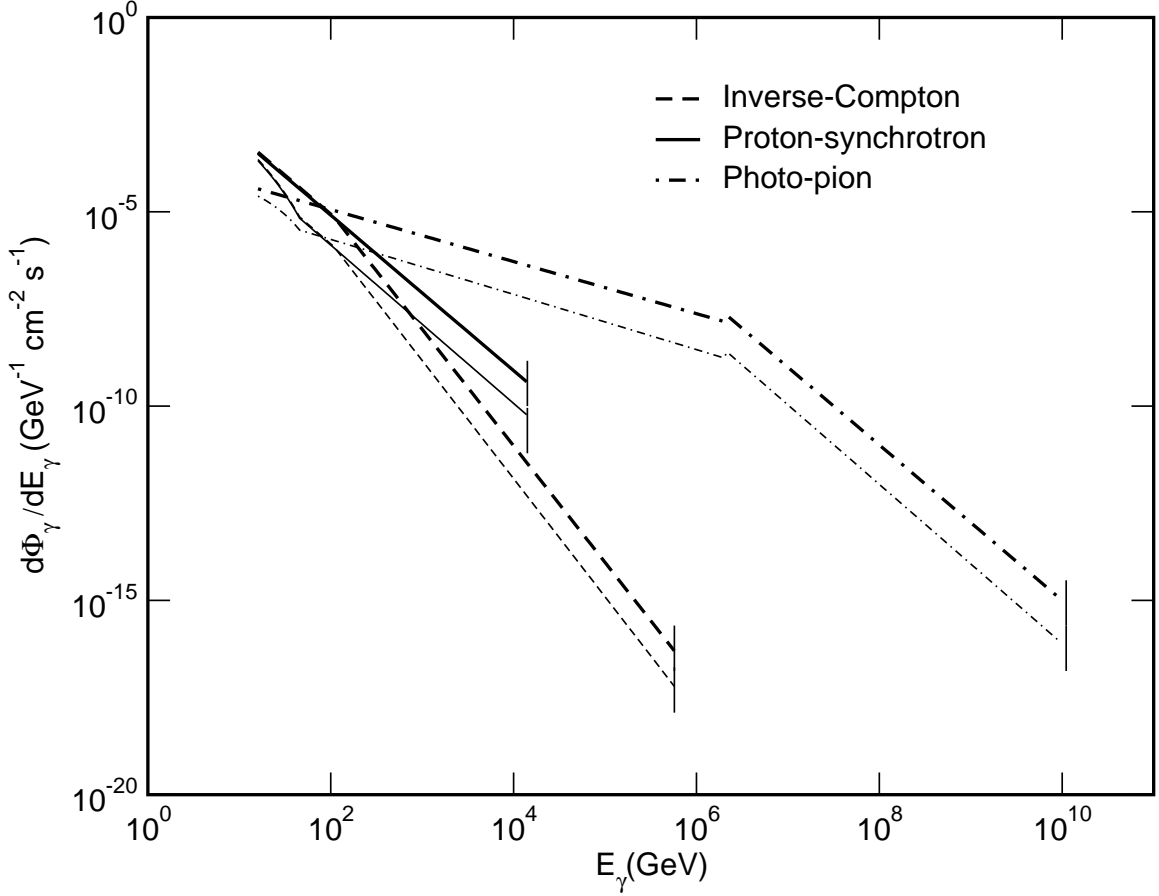


FIG. 1: Illustrative gamma-ray spectra for the three models discussed in the text. Spectra have been normalized to produce the muon excess observed by Project *GRAND* for GRB 971110. The curves begin at the detection threshold for Project *GRAND* and run to the respective cut-offs of each model. The thick lines are the raw source spectra. The thin lines illustrate the effects of internal pair-production optical depth on the source spectra. The change in energy dependence of the internal optical depth is apparent above about 50 GeV.

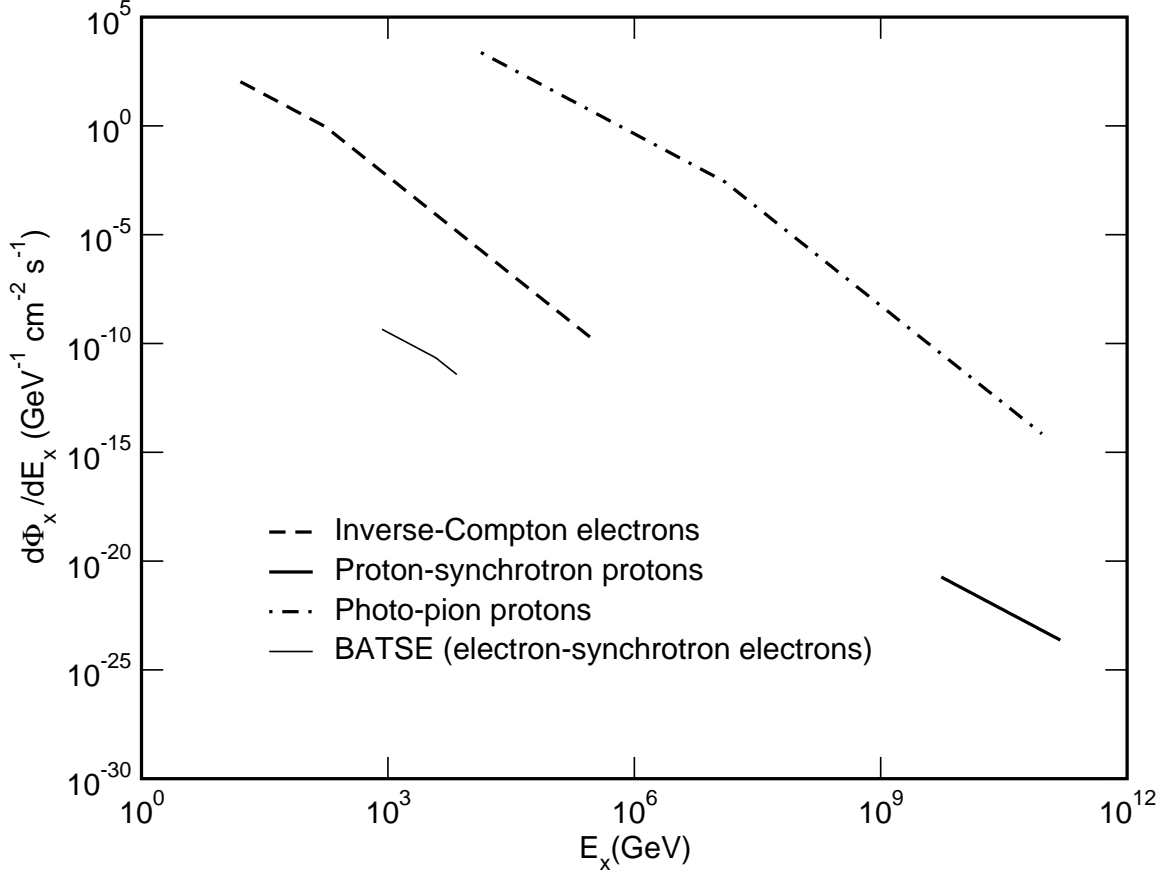


FIG. 2: Illustrative electron and proton spectra in the source frame for the three models discussed in the text. Spectra have been normalized to produce the muon excess observed by Project *GRAND* or to fit the observed *BATSE* spectrum for GRB 971110.

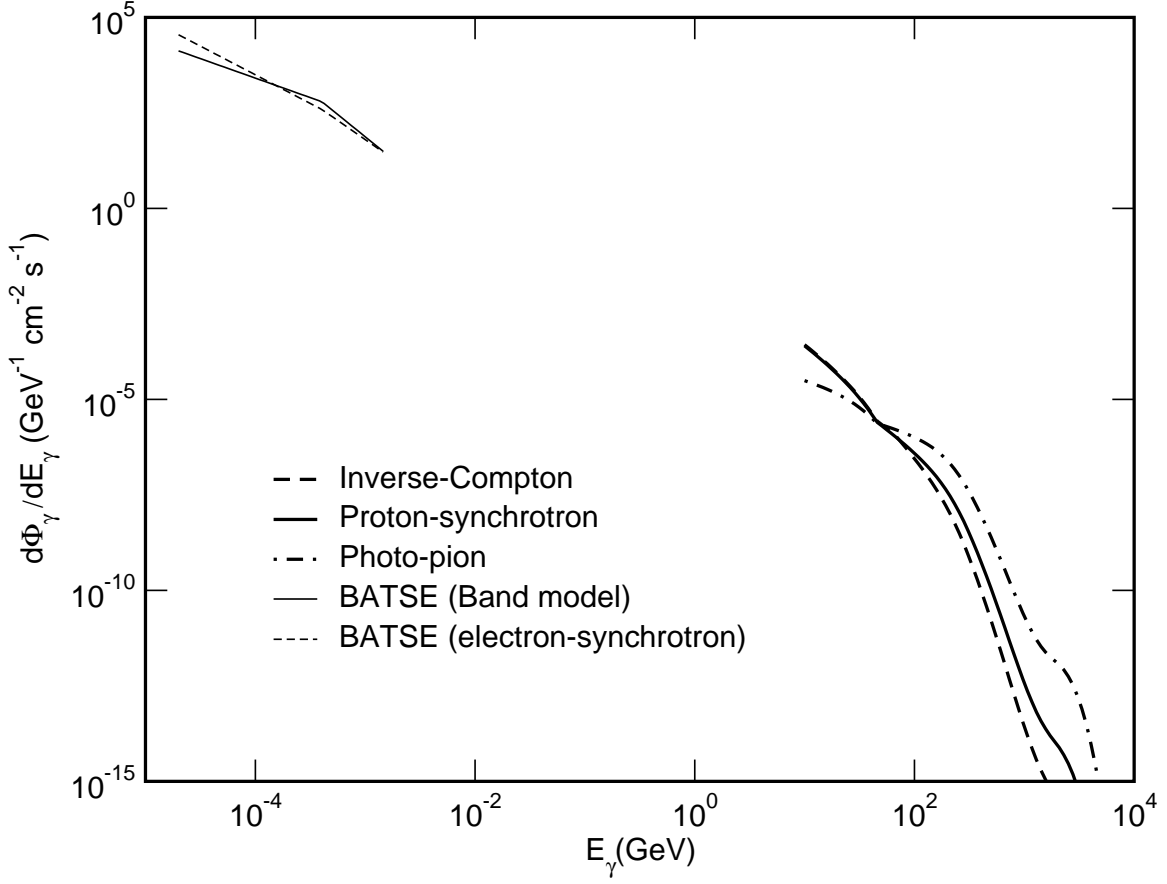


FIG. 3: Illustration of the effects of internal and intergalactic pair-production optical depth on the source spectra shown in Figure 1. This calculation assumes that the source (GRB 971110) is at a redshift of  $z = 0.6$ . The change in energy dependence of the internal optical depth is apparent above about 50 GeV. For illustration, this plot also includes the observed *BATSE* spectrum for this burst, fit with both the Band (Eq. [1]) and electron-synchrotron models.

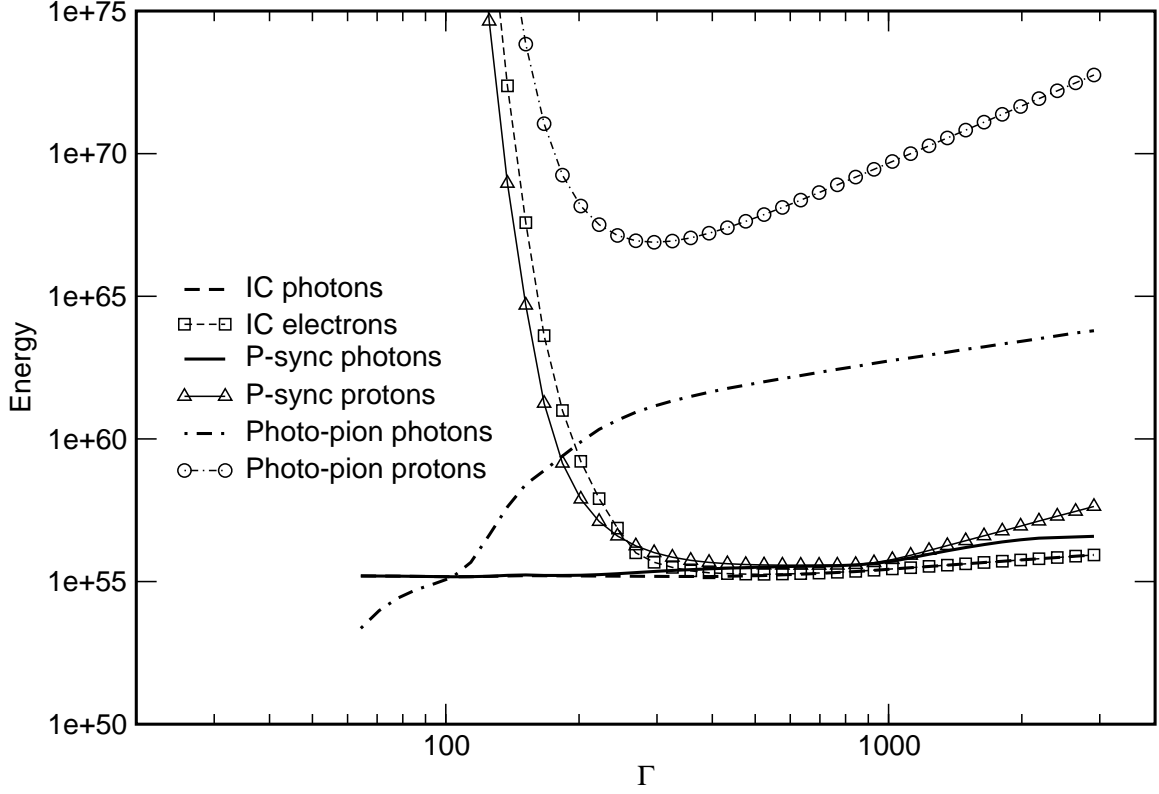


FIG. 4: Plot of the energy escaping in gamma rays (accounting for  $\tau_{\gamma\gamma,int}$ ) and the source energy in protons or electrons for the inverse-Compton, proton-synchrotron, and photo-pion models as a function of the Lorentz boost of the GRB fireball. These curves correspond to spectra that were normalized to fit the observed muon excess for GRB 971110. The sharp increase in the energy content of the protons and electrons at small  $\Gamma$  enters primarily through the internal optical depth.

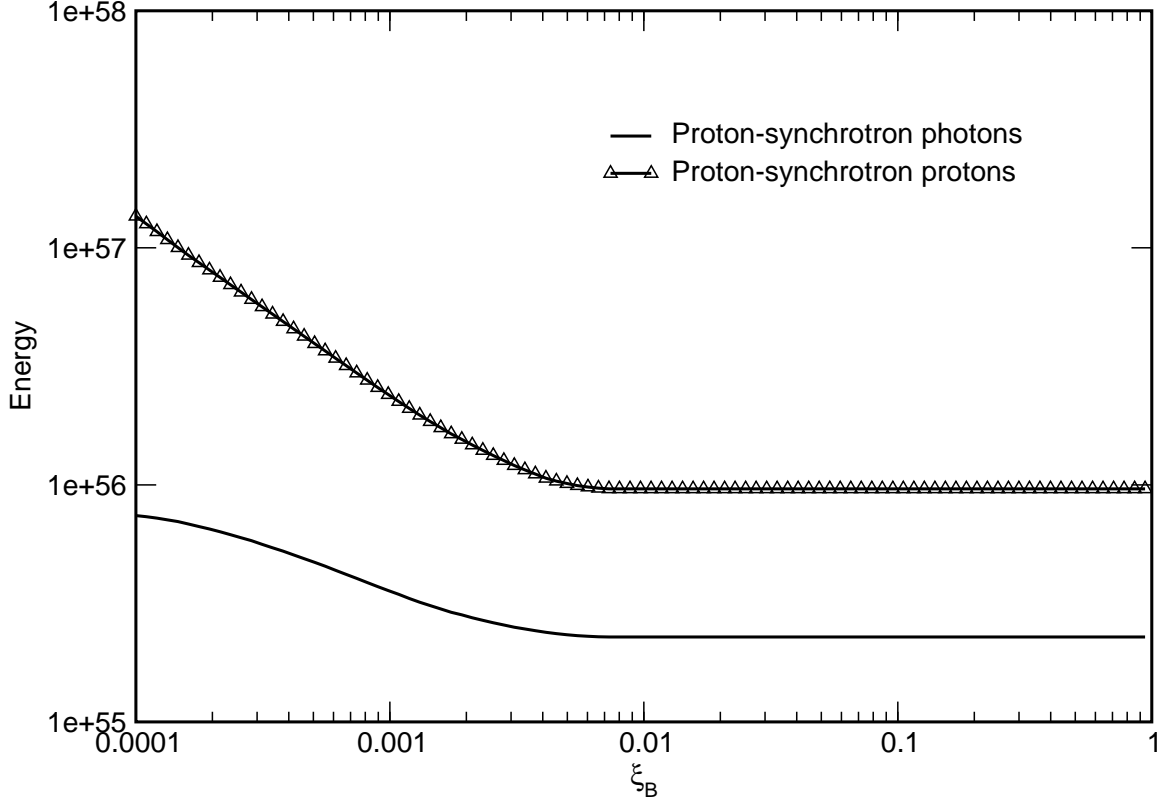


FIG. 5: Plot of the energy escaping in gamma rays (accounting for  $\tau_{\gamma\gamma,int}$ ) and the source energy in protons for the proton-synchrotron model as a function of the magnetic equipartition of the GRB fireball. These curves correspond to spectra that were normalized to fit the observed muon excess for GRB 971110. The offset between the photon and proton spectra for  $\xi_B \gtrsim 0.01$  is due solely to absorption due to the internal optical depth,  $\tau_{\gamma\gamma,int}$ .

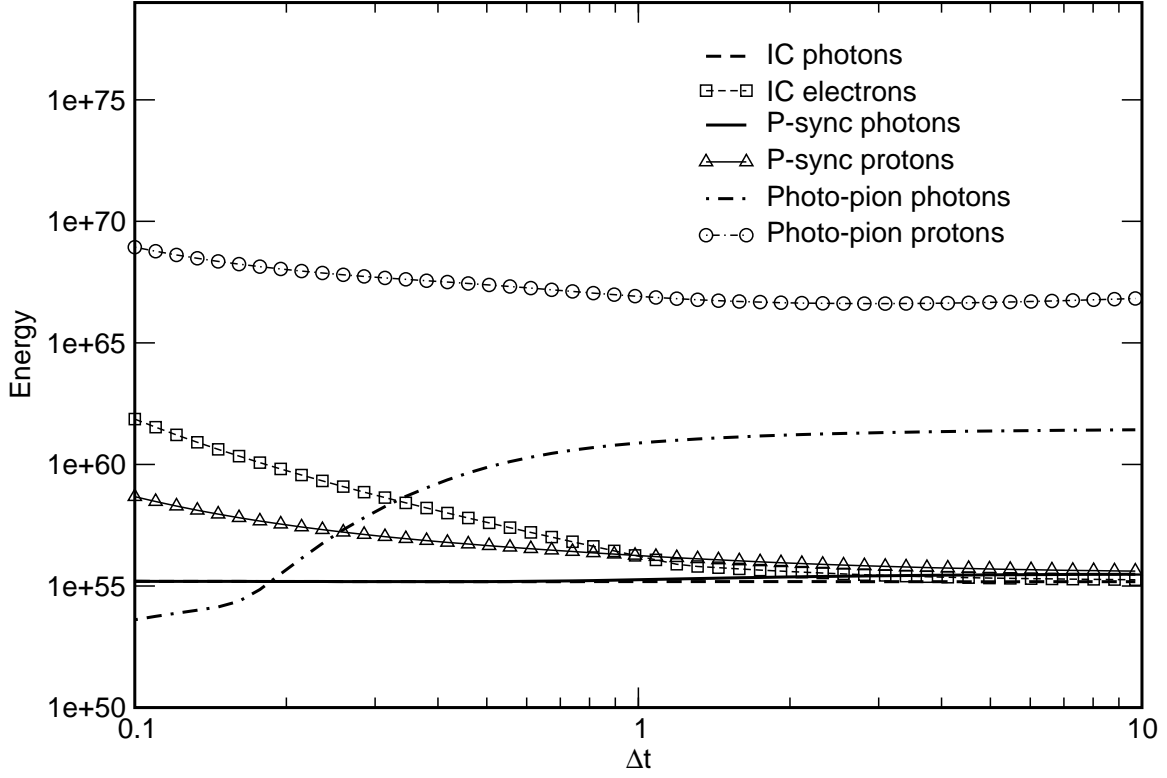


FIG. 6: Plot of the energy escaping in gamma rays (accounting for  $\tau_{\gamma\gamma,int}$ ) and the source energy in protons or electrons for the inverse-Compton, proton-synchrotron, and photo-pion models as a function of the time variability of the GRB fireball. These curves correspond to spectra that were normalized to fit the observed muon excess for GRB 971110.

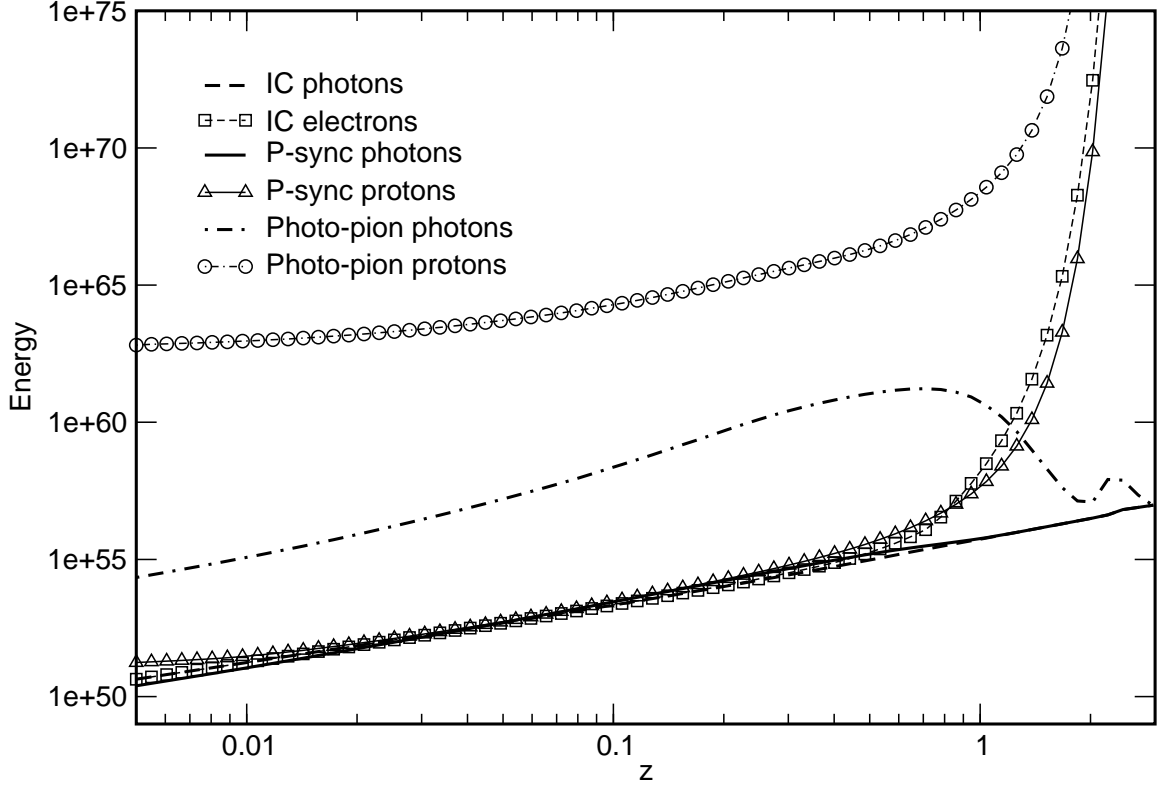


FIG. 7: Plot of the energy escaping in gamma rays (accounting for  $\tau_{\gamma\gamma,int}$ ) and the source energy in protons or electrons for the inverse-Compton, proton-synchrotron, and photo-pion models as a function of the redshift of the GRB fireball. These curves correspond to spectra that were normalized to fit the observed muon excess for GRB 971110.



TABLE I: Project *GRAND*'s Response to Selected *BATSE* Bursts

GRB	Trig	T90 <sup>a</sup>	RA <sup>a</sup>	Dec <sup>a</sup>	$\delta\theta^a$	$N_\mu^b$
971110	6472	195.2	242	50	0.6	$467 \pm 171$
990123	7343	62.5	229	42	0.4	$< 75$
940526	2994	48.6	132	34	1.7	$< 76$
980420	6694	39.9	293	27	0.6	$< 133$
960428	5450	172.2	304	35	1.0	$< 213$
980105	6560	36.8	37	52	1.4	$< 107$
980301	6619	36.0	148	35	1.3	$< 150$
970417a	6188	7.9	290 <sup>c</sup>	54 <sup>c</sup>	0.5 <sup>c</sup>	$20 \pm 17$

<sup>a</sup>Angles RA, Dec, and  $\delta\theta$  in degrees and T90 in seconds.

<sup>b</sup>Upper limits are  $2\sigma$  confidence level.

<sup>c</sup>RA, Dec, and  $\delta\theta$  for GRB 970417a are based upon the *Milagrito* data.

TABLE II: Observed and Inferred GRB Properties in *BATSE* Energy Range

GRB	$a$ ( $\text{cm}^{-2} \text{ s}^{-1} \text{ MeV}^{-1}$ )	$\beta_l$	$\beta_h$	$\epsilon_{\gamma b}^{ob}$ (MeV)	$\Delta t$ (s)
971110	$0.0751 \pm 0.0095$	$1.02 \pm 0.04$	$2.33 \pm 0.11$	$0.404 \pm 0.041$	1.8
990123	$1.93 \pm 0.14$	$0.60 \pm 0.01$	$3.11 \pm 0.07$	$1.29 \pm 0.07$	4.1
940526	$\leq 0.217$	$1.01 \pm 0.02$	$> 3.2$	$> 1.28$	1.2
980420	$0.0815 \pm 0.0105$	$0.18 \pm 0.08$	$2.57 \pm 0.27$	$0.553 \pm 0.033$	1.8
960428	$0.0610 \pm 0.0086$	$0.58 \pm 0.09$	$2.49 \pm 0.24$	$0.433 \pm 0.033$	0.7
980105	$0.0332 \pm 0.0081$	$0.69 \pm 0.06$	$2.82 \pm 0.19$	$0.286 \pm 0.031$	1.2
980301	$0.0068 \pm 0.0020$	$0.54 \pm 0.20$	$3.26 \pm 1.41$	$0.317 \pm 0.033$	2.3
970417a	$0.0100 \pm 0.0061^a$	$1.0 \pm 0.5^b$	$2.25 \pm 0.75^b$	$0.250 \pm 0.150^b$	1.1

<sup>a</sup>Spectral fits were not available for GRB 970417a. Properties are based upon assumed redshift  $z \approx 0.7$ , observed *BATSE* fluence, and average GRB spectral shape.

<sup>b</sup>Average parameters for all bright GRBs considered in Preece et al. (2000).

TABLE III: Variability-Luminosity Redshift Estimates

GRB	$V$	$P_{256}^a$ (photons $\text{cm}^{-2} \text{s}^{-1}$ )	$z^b$	$L_{256}^c$ (erg $\text{s}^{-1}$ )	$L_\gamma^c$ (erg $\text{s}^{-1}$ )
971110	0.0204	$17.4 \pm 0.2$	$0.6 \pm 0.2$	$(6.6 \pm 5.2) \times 10^{51}$	$(3.8 \pm 2.1) \times 10^{50}$
990123	0.0113	$16.6 \pm 0.2$	$1.6^d$	$(6.6 \pm 1.0) \times 10^{52}$	$(7.8 \pm 2.6) \times 10^{51}$
940526	0.0175	$14.4 \pm 0.3$	$0.6 \pm 0.2$	$(5.5 \pm 4.3) \times 10^{51}$	$(1.8 \pm 0.7) \times 10^{50}$
980420	0.0267	$3.7 \pm 0.1$	$1.1 \pm 0.3$	$(7.2 \pm 4.8) \times 10^{51}$	$(1.0 \pm 0.4) \times 10^{51}$
960428	0.0628	$4.2 \pm 0.1$	$1.6 \pm 0.5$	$(1.9 \pm 1.4) \times 10^{52}$	$(2.5 \pm 1.1) \times 10^{51}$
980105	0.0671	$10.6 \pm 0.2$	$1.2 \pm 0.4$	$(2.4 \pm 1.9) \times 10^{52}$	$(1.2 \pm 0.7) \times 10^{51}$
980301	0.0232	$0.9 \pm 0.1$	$2.4 \pm 0.8$	$(9.8 \pm 5.7) \times 10^{51}$	$(2.6 \pm 5.0) \times 10^{51}$
970417a <sup>e</sup>	...	$0.7 \pm 0.1$	$0.7 \pm 0.2^f$	$(4.3 \pm 3.1) \times 10^{50}$	$(0.2 \pm 1.4) \times 10^{51}$

<sup>a</sup>Available at <http://www.batse.msfc.nasa.gov/batse/>

<sup>b</sup>The redshift uncertainties are crudely estimated as  $z/3$  from the variability-luminosity relation.

<sup>c</sup>We quote the isotropic luminosities. These must be multiplied by  $\Omega/(4\pi)$  to get the true luminosities.

<sup>d</sup>Kulkarni et al. (1999)

<sup>e</sup>GRB 970417a was too weak in the *BATSE* band to apply the variability-luminosity relation.

<sup>f</sup>Totani (2000).

TABLE IV: Internal & Intergalactic Optical Depths

GRB	Internal Optical Depth		Intergalactic Optical Depth	
	$E_\gamma = 100 \text{ GeV}$	1 TeV	$E_\gamma = 100 \text{ GeV}$	1 TeV
971110	$2.7 \pm 3.5$	$2.9 \pm 3.6$	$0.4 \pm 0.2$	$9.6 \pm 4.0$
990123	... <sup>a</sup>	... <sup>a</sup>	2.8	31.
940526	... <sup>a</sup>	... <sup>a</sup>	$0.4 \pm 0.2$	$9.6 \pm 4.0$
980420	... <sup>a</sup>	... <sup>a</sup>	$1.3 \pm 0.8$	$20. \pm 6.$
960428	... <sup>a</sup>	... <sup>a</sup>	$3.1 \pm 2.0$	$30. \pm 10.$
980105	... <sup>a</sup>	... <sup>a</sup>	$1.6 \pm 1.2$	$22. \pm 8.$
980301	... <sup>a</sup>	... <sup>a</sup>	$6.8 \pm 3.4$	$44. \pm 13.$
970417a	... <sup>a</sup>	... <sup>a</sup>	$0.5 \pm 0.3$	$12. \pm 4.$

<sup>a</sup>Large uncertainties in the fit parameters made constraints on the internal optical depth uninformative in these cases. For these bursts, we have made the optimistic assumption  $\tau_{\gamma\gamma,int} = 0$ .

TABLE V: Inferred Properties of Inverse-Compton Model

GRB	$A_{\gamma}^{IC}$ ( $\text{cm}^{-2} \text{s}^{-1} \text{GeV}^{-1}$ )	$E_{cool}^{ob}$ (GeV)	$E_{KN}^{ob}$ (GeV)	$E_{cool}^{KN,ob}$ (GeV)	$E_{\gamma}^{Tot,IC}{}^a$ (erg)	$E_e^{Tot,IC}{}^a$ (erg)
971110	$4. \pm 80.$	$(1. \pm 13.) \times 10^7$	$25. \pm 7.$	$75. \pm 48.$	$(2.6 \pm 8.6) \times 10^{55}$	$(1. \pm 15.) \times 10^{60}$
990123	$< 6.2 \times 10^{-2}$	0.04	2.8	23.	$< 3.5 \times 10^{55}$	$< 2.6 \times 10^{57}$
940526	$< 1.2 \times 10^{-2}$	14.	7.3	5.1	$< 2.5 \times 10^{54}$	$< 2.5 \times 10^{54}$
980420	$< 4.2 \times 10^{-2}$	0.3	9.8	56.	$< 2.4 \times 10^{55}$	$< 1.6 \times 10^{56}$
960428	$< 1.7 \times 10^{-2}$	0.004	8.2	380	$< 2.0 \times 10^{56}$	$< 2.4 \times 10^{59}$
980105	$< 9.6 \times 10^{-2}$	0.04	17.	350	$< 3.9 \times 10^{55}$	$< 1.4 \times 10^{57}$
980301	$< 2.1 \times 10^{-1}$	0.05	6.5	73.	$< 3.4 \times 10^{56}$	$< 1.0 \times 10^{58}$
970417a	$< 1.3 \times 10^{-2}$	8.6	33.	63.	$< 2.8 \times 10^{54}$	$< 2.8 \times 10^{54}$

Here we estimate the total energy escaping in the gamma-ray component from each burst using the inverse-Compton model. We also estimate the total energy in the electron component at the source.

<sup>a</sup>We quote the isotropic energies. These entries must be multiplied by  $\Omega/(4\pi)$  to get the true energies.

TABLE VI: Inferred Properties of Proton-Synchrotron Model

GRB	$A_p^{p-sync}$ ( $\text{cm}^{-2} \text{s}^{-1} \text{GeV}^{-1}$ )	$E_{\gamma b}^{ob}$ (GeV)	$E_{\gamma}^{Tot,p-sync}{}^a$ (erg)	$E_p^{Tot,p-sync}{}^a$ (erg)
971110	$1. \pm 22.$	$(1. \pm 22.) \times 10^2$	$(3. \pm 10.) \times 10^{55}$	$(1. \pm 21.) \times 10^{58}$
990123	$< 1.9 \times 10^{-2}$	$6.2 \times 10^{-5}$	$< 9.6 \times 10^{55}$	$< 9.6 \times 10^{55}$
940526	$< 1.4 \times 10^{-2}$	$1.3 \times 10^{-2}$	$< 5.3 \times 10^{54}$	$< 5.3 \times 10^{54}$
980420	$< 4.1 \times 10^{-2}$	$8.9 \times 10^{-4}$	$< 5.4 \times 10^{55}$	$< 5.4 \times 10^{55}$
960428	$< 2.0 \times 10^{-2}$	$5.8 \times 10^{-5}$	$< 2.7 \times 10^{56}$	$< 2.7 \times 10^{56}$
980105	$< 3.8 \times 10^{-2}$	$4.0 \times 10^{-4}$	$< 5.6 \times 10^{55}$	$< 5.6 \times 10^{55}$
980301	$< 9.3 \times 10^{-2}$	$2.5 \times 10^{-4}$	$< 7.0 \times 10^{56}$	$< 7.0 \times 10^{56}$
970417a	$< 6.7 \times 10^{-2}$	$3.0 \times 10^{-2}$	$< 5.9 \times 10^{54}$	$< 5.9 \times 10^{54}$

Here we estimate the total energy escaping in the gamma-ray component from each burst using the proton-synchrotron model. We also estimate the total energy in the proton component at the source.

<sup>a</sup>We quote the isotropic energies. These entries must be multiplied by  $\Omega/(4\pi)$  to get the true energies.

TABLE VII: Inferred Properties of Photo-Pion Model

GRB	$A_p^\pi$ ( $\text{cm}^{-2} \text{ s}^{-1} \text{ GeV}^{-1}$ )	$E_{\gamma b}^{ob}$ ( $10^5 \text{ GeV}$ )	$E_\gamma^{Tot,\pi}{}^a$ (erg)	$E_p^{Tot,\pi}{}^a$ (erg)
971110	$(1. \pm 13.) \times 10^{11}$	$13. \pm 4.$	$(4. \pm 27.) \times 10^{61}$	$(2. \pm 27.) \times 10^{69}$
990123	$< 1.3 \times 10^{20}$	1.5	$< 1.2 \times 10^{74}$	$< 1.1 \times 10^{78}$
940526	$< 1.8 \times 10^{13}$	4.0	$< 2.0 \times 10^{65}$	$< 1.3 \times 10^{70}$
980420	$< 7.8 \times 10^{15}$	5.3	$< 2.5 \times 10^{69}$	$< 2.1 \times 10^{73}$
960428	$< 3.9 \times 10^{18}$	4.4	$< 5.3 \times 10^{73}$	$< 1.1 \times 10^{77}$
980105	$< 2.3 \times 10^{17}$	9.4	$< 1.8 \times 10^{71}$	$< 7.8 \times 10^{74}$
980301	$< 3.1 \times 10^{27}$	3.5	$< 3.4 \times 10^{81}$	$< 4.8 \times 10^{85}$
970417a	$< 5.8 \times 10^{12}$	18.	$< 3.2 \times 10^{64}$	$< 1.2 \times 10^{69}$

Here we estimate the total energy escaping in the gamma-ray component from each burst using the photo-pion model. We also estimate the total energy in the proton component at the source.

<sup>a</sup>We quote the isotropic energies. These entries must be multiplied by  $\Omega/(4\pi)$  to get the true energies.